C. R. Physique 12 (2011) 446–460

Contents lists available at ScienceDirect

Comptes Rendus Physique

www.sciencedirect.com

Superconductivity of strongly correlated systems / Supraconductivité des systèmes fortement corrélés

Quantum oscillations and the Fermi surface of high-temperature cuprate superconductors

Oscillations quantiques et la surface de Fermi des supraconducteurs de cuprates à haute température

Baptiste Vignolle [a], David Vignolles [a], David LeBoeuf [a], Stéphane Lepault [a], Brad Ramshaw [b], Ruixing Liang [b,e], D.A. Bonn [b,e], W.N. Hardy [b,e], Nicolas Doiron-Leyraud [d], A. Carrington [c], N.E. Hussey [c], Louis Taillefer [d,e], Cyril Proust [a,e,*]

[a] *Laboratoire National des Champs Magnétiques Intenses (CNRS-INSA-UJF-UPS), 143, avenue de Rangueil, 31400 Toulouse, France*
[b] *Department of Physics and Astronomy, University of British Columbia, Vancouver, British Columbia, V6T 1Z1, Canada*
[c] *H. H. Wills Physics Laboratory, University of Bristol, Tyndall Avenue, Bristol BS8 1TL, UK*
[d] *Département de physique and RQMP, Université de Sherbrooke, Sherbrooke, Québec J1K 2R1, Canada*
[e] *Canadian Institute for Advanced Research, Toronto, Ontario M5G 1Z8, Canada*

ARTICLE INFO

Article history:
Available online 25 May 2011

Keywords:
High temperature superconductors
Quantum oscillations
Fermi surface

Mots-clés :
Supraconductivité à haute température
Oscillations quantiques
Surface de Fermi

ABSTRACT

Over 20 years since the discovery of high temperature superconductivity in cuprates (Bednorz and Müller, 1986 [1]), the first convincing observation of quantum oscillations in underdoped $YBa_2Cu_3O_{6.5}$ (Doiron-Leyraud et al., 2007 [2]) has deeply changed the theoretical landscape relevant to these materials. The Fermi surface is a basic concept of solid state physics, which underpins most physical properties (electrical, thermal, optical, etc.) of a metal. Even in the presence of interactions, this fundamental concept remains robust. While there was little doubt about the existence of a Fermi surface on the overdoped side of the phase diagram of the cuprates, the discovery of quantum oscillations in the underdoped regime was a surprise. The small pockets inferred from the measurements in underdoped $YBa_2Cu_3O_y$ contrast with the large orbit found in overdoped $Tl_2Ba_2CuO_{6+\delta}$. A central issue in understanding the phase diagram of high temperature superconductors is the origin of this difference at opposite sides of the superconducting dome. This review aims to shed light on this issue by bringing together recent results of quantum oscillation and transport measurements under high magnetic fields in hole-doped cuprates.

RÉSUMÉ

Près de 20 ans après la découverte de la supraconductivité à haute température dans les cuprates (Bednorz et Müller, 1986 [1]), les bases théoriques nécessaires à la compréhension de ces systèmes ont été bouleversées par les premières observations indiscutables d'oscillations quantiques dans $YBa_2Cu_3O_{6.5}$ sous-dopé (Doiron-Leyraud et al., 2007 [2]). En effet, la surface de Fermi reflète la plupart des propriétés physiques des métaux (électriques, thermiques, optiques, etc.). Ce concept de base est très robuste, et demeure valide même en présence de fortes interactions électroniques. Néanmoins, s'il n'y avait

* Corresponding author.
E-mail address: cyril.proust@lncmi.cnrs.fr (C. Proust).

1631-0705/$ – see front matter
doi:10.1016/j.crhy.2011.04.011

aucun doute sur l'existence de cette surface de Fermi du côté sur-dopé, la découverte d'oscillations quantiques du côté sous-dopé a été, elle, une vraie surprise. Les petites poches déduites des mesures dans $YBa_2Cu_3O_y$ sous-dopé contrastent avec la grande orbite observée dans $Tl_2Ba_2CuO_{6+\delta}$ sur-dopé. Une question clef posée par le diagramme de phase des cuprates est donc cette différence de comportement de part et d'autre du dôme supraconducteur. Nous apportons des éléments de réponse à cette question, à la lumière des résultats récents obtenus par les mesures d'oscillations quantiques et de transport sous fort champ magnétique dans les cuprates dopés aux trous.

1. Introduction

The generic phase diagram of hole-doped cuprates shown in Fig. 1 shows that high temperature superconductivity (HTSC) [1] is sandwiched between an insulating and a metallic phase. At zero doping, band structure calculations predict the conducting band to be half-filled and therefore the system to be metallic. However, the strong electron–electron correlations (strong on-site Coulomb repulsion) impede electrons from hopping from one atom to another. The resulting ground state is a Mott insulator, which adopts an antiferromagnetic (AF) configuration for the Cu spin 1/2. The AF phase is rapidly destabilized when carriers are added in the CuO_2 planes and the Néel temperature T_N vanishes at $p \approx 0.05$ where the superconducting dome emerges and extends to $p \approx 0.31$ (for overdoped $Tl_2Ba_2CuO_{6+\delta}$). The optimal doping corresponds to $p \approx 0.16$ where the superconducting transition T_c is maximal. The underdoped (overdoped) regime corresponds to the left (right) part of the dome.

On the strongly overdoped side, the electronic properties can be understood within the framework of the generalized Fermi-liquid (FL) theory, the standard theory of electrons in solids. One robust signature of a FL is the observation of the Wiedemann–Franz law in overdoped $Tl_2Ba_2CuO_{6+\delta}$ [3] which demonstrates that the fermions which carry heat also carry charge e and are therefore indistinguishable from standard Landau quasiparticles. Another strong indication of FL behaviour comes from transport measurements in heavily overdoped (non-superconducting) $La_{2-x}Sr_xCuO_4$ which shows that both ρ_{ab} and ρ_c exhibit strictly T^2 behavior below 50 K [4]. However, as the overdoped compound becomes superconducting, an additional T-linear component of the resistivity appears as seen in resistivity [3,5,6] and angular magneto-resistance oscillation (AMRO) [7] measurements on $Tl_2Ba_2CuO_{6+\delta}$ and in high-field magneto-transport measurements in the normal state of overdoped $La_{1.6-x}Nd_{0.4}Sr_xCuO_4$ [8] and $La_{2-x}Sr_xCuO_4$ [9].

The underdoped side of the phase diagram is characterized by the presence of the mysterious *pseudogap* phase. The first evidence of the pseudogap phase came from NMR measurements back in 1989 [10,11]. At a temperature $T^* \approx 300$ K, a sudden suppression of the Knight shift occurs. The fact that this happens at a temperature much higher than T_c in underdoped cuprates suggests that the pseudogap is associated with spin singlet formation in agreement with a scenario based on preformed pairs which form at T^* but without phase coherence. The latter occurs only at T_c where superconductivity (zero resistance, Meissner effect) sets in. Angle-resolved photoemission spectroscopy (ARPES) measurements in underdoped $Bi_2Sr_2CaCu_2O_{8+\delta}$ close to the anti-nodal directions have revealed that the quasiparticle peak disappears above T_c and that there is an energy gap above T_c which persists up to T^* [12]. This gap is strongly anisotropic since it appears only at the anti-nodal region of the Fermi surface (FS). The d-wave node below T_c becomes a gapless arc above T_c which expands with increasing temperature to form the full FS at T^*. The similarity between the superconducting gap and the pseudogap suggests that the latter may be a precursor of the former.

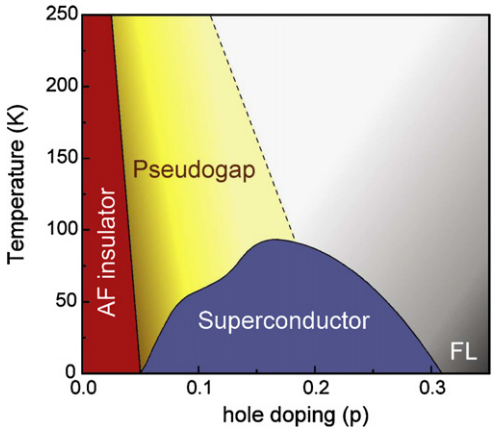

Fig. 1. Generic temperature-doping phase diagram of high temperature cuprate superconductors. The parent compound is an antiferromagnetic Mott insulator. The dotted line is a crossover which mark the appearance of the pseudogap phase. At high doping, a generalized Fermi liquid behavior is recovered.

An alternative scenario for the pseudogap phase is to assume that T^* marks the onset of an ordered phase. Coming back to the NMR measurements and assuming that the Knight shift is proportional to the density of states at the Fermi level, T^* marks the onset of an instability resulting in an energy gap. At least three experiments suggest that T^* marks the onset of a phase with broken symmetry: using polarized elastic neutron diffraction, a novel AF order at $Q = 0$ has been identified in underdoped $YBa_2Cu_3O_y$ [13] and in underdoped $HgBa_2CuO_{4+\delta}$ [14]. Polar Kerr effect measurements in underdoped $YBa_2Cu_3O_y$ found also evidence for broken time-reversal symmetry near the pseudogap temperature [15]. Finally, recent Nernst effect measurements in underdoped $YBa_2Cu_3O_y$ report the observation of a large in-plane anisotropy of the Nernst coefficient that sets in precisely at T^*, suggesting that the pseudogap phase is an electronic state that breaks four-fold rotational symmetry [16].

There is still no consensus whether the pseudogap is a precursor to or distinct from the superconducting phase [17]. In most doped Mott insulator scenarios such as the "resonating valence bond" (RVB) [18] or the pre-formed pairs scenario [19], the pseudogap phase corresponds to a phase with either spin singlets formation or pre-formed pairs without phase coherence. The FS consists of 4 nodal hole pockets, with one side of each pocket having a quasiparticle residue much smaller than the other one, leading to Fermi arcs. In other classes of scenarios such as spin density wave order [20,21], stripe order [22,23], d-density wave order [24] or Marginal Fermi liquid (MFL) [25], the pseudogap is not related to superconductivity but rather competes with it. All these scenarios predict a quantum critical point lying inside the superconducting dome in the overdoped side [26,27] where the pseudogap disappears. Except for the MFL scenario, they involve a FS reconstruction where the resulting FS typically consists of electron and hole sheets.

The discovery of magnetic quantum oscillations in underdoped $YBa_2Cu_3O_y$ in 2007 has provided us with a powerful new probe of this reconstruction [2].

2. Magnetic quantum oscillations

2.1. Theory

In the presence of a magnetic field, the energy levels of electrons are quantized into Landau levels. A full quantum mechanic treatment leads to the electronic dispersion for free electrons:

$$\varepsilon_n(k_z) = \left(n + \frac{1}{2}\right)\hbar\omega_c + \frac{\hbar^2 k_z^2}{2m}$$

The Landau levels are separated by the energy $\hbar\omega_c = \hbar eB/m^*$, which increases as the field increases. As the field is swept, there is a reorganization of the electronic states: each time a Landau level crosses the Fermi energy, there is a singularity in the density of states which gives rise to the oscillation of many physical properties [28]. The oscillation of the magnetization is called the de Haas–van Alphen effect [29] (dHvA) and the oscillation of the resistivity is called the Shubnikov–de Haas effect [30] (SdH) in tribute to the scientists who discovered these effects in elemental bismuth in 1930. The dHvA and SdH effects are described by the Lifshitz–Kosevich (LK) theory [31]. The oscillatory part of the magnetoconductivity for a general 3D case is given by:

$$\frac{\Delta\sigma}{\sigma} \propto \sum_i A_i^0 B^{\frac{1}{2}} \sum_{p=1}^{\infty} R_T R_D R_S \cos\left(2\pi p\left[\frac{F_i}{B} - \gamma_i\right] \pm \frac{\pi}{4}\right) \tag{1}$$

The frequency F_i of the oscillation is proportional to the extremal area A_i of the FS (sum over i Fermi surfaces): $F_i = \frac{\hbar}{2\pi e} A_i$. The index p corresponds to the sum over the harmonics. γ_i is a phase factor and R_T, R_D and R_S are the thermal, impurity and spin damping factors, respectively.

When the amplitude of the oscillations is small in comparison to the background, the LK formula can be applied to the oscillatory part of the magnetoresistance: $\frac{\Delta\sigma}{\sigma} \approx \frac{\Delta\rho}{\rho}$. When the amplitude of the oscillations becomes comparable to the background, then one has to work on the oscillatory part of the conductivity. Dividing the oscillatory part by the background and applying the LK formula for large amplitude oscillations would generally lead to the appearance of harmonics in the signal.

In order to observe quantum oscillations, it is necessary that the distance between Landau levels is greater than the thermal broadening, e.g. $\hbar\omega_c > k_B T$. These measurements are therefore performed at low temperature (below 10 K in the case of the cuprates). The damping factor

$$R_T = \frac{\alpha T m_i^*/B}{\sinh(\alpha T m_i^*/B)} = \frac{X}{\sinh(X)}$$

with $\alpha = 2\pi^2 m^* k_B/e\hbar$ takes into account finite temperature effects due to the broadening of the Fermi function. It allows the effective mass m^* to be deduced from the temperature dependence of the amplitude of the oscillations. m^* is the thermodynamic effective mass which includes electron–electron and electron–phonon interactions and can be compared to that deduced from the Sommerfeld coefficient of the specific heat.

Another requirement to observe quantum oscillations is that the broadening of the Landau levels due to impurity scattering should be less than the distance between the Landau levels, e.g. $\hbar\omega_c > \hbar/\tau$ leading to $\omega_c\tau > 1$. The damping

factor

$$R_D = \exp\left(-\pi\sqrt{\frac{2\hbar F_0}{e}}\frac{1}{\ell B}\right)$$

is called the Dingle factor, where ℓ is the low temperature mean free path that can be deduced from the field dependence of the amplitude of the oscillations. This term imposes the necessity to work on high quality single crystals. Due to the stronger effect of small angle scattering on the dephasing of the quantum oscillations, ℓ extracted from quantum oscillations is usually smaller than the mean free path deduced from transport measurements [32].

Finally, the damping factor $R_S = \cos(\frac{\pi g l m_s}{2m_0})$ takes into account the spin splitting due to Zeeman effect. The effective mass which enters this expression is usually not the same as m^*. Since m_s only includes electro-electron interactions: $m^* = (1+\lambda_{\text{phonon}})m_s$ [33].[1]

In the case of a quasi-2D metal, the warping of the FS manifests itself as a frequency-splitting corresponding to neck and belly frequencies, associated with the minimum and maximum cross-sections of the FS. The oscillatory part of the magnetoresistivity of the fundamental component of oscillation becomes:

$$\frac{\Delta\rho}{\rho} \propto A_0 R_T R_D R_s J_0\left[2\pi\frac{\Delta F}{B\cos\theta}J_0(k_F c\tan\theta)\right]\cos\left[2\pi\left(\frac{F}{B\cos\theta}-\gamma\right)\right] \tag{2}$$

F is the frequency corresponding to the average area of a cylinder, ΔF is the splitting corresponding to the warping of the cylinder described by the Bessel function J_0, k_F is the average radius of the cylinder, c is the c-axis lattice parameter, θ is the angle between the field and the c-axis, γ is a phase factor. R_T, R_D, and R_s are the damping factors discussed previously. Instead of treating the electron effective mass, the amplitude, the phase of the oscillations, and the Dingle temperature separately for the neck and belly orbits, only one value of each of these parameters is required to describe a single FS, reducing the number of fitting parameters.

2.2. Experimental techniques

Transport and torque measurements up to 60 T are routinely performed at the LNCMI in Toulouse, in pulsed resistive magnets driven by a 24 kV, 14 MJ capacitor bank [35]. Variable temperatures are obtained using a standard ^{4}He cryostat for T varying from 1.5 to 300 K and using a dilution fridge with a plastic mixing chamber for temperatures below 1.5 K. For in-plane transport measurements, longitudinal (R_{xx}) and transverse (R_{xy}) resistances are obtained from the voltage difference measured diagonally on either side of the sample width, for a field parallel (up) and anti-parallel (down) to the c-axis. Electrical contacts to the sample were made by evaporating gold pads. For longitudinal c-axis transport ($I \parallel B \parallel c$), large current pads and small voltage pads mounted across the top and bottom so as to short out any in-plane current (Corbino geometry). A current excitation of 5 to 10 mA at 60 kHz was used. Typical dimension of the samples are ($1\times1\times0.05$ mm^3).

Torque measurements were performed with a commercial piezoresistive microcantilever [36] down to 0.4 K. The sample was glued with Araldite epoxy to the cantilever. A one-axis rotating sample holder allowed the angle ($\theta \sim 5°$) to be varied between the normal to the CuO_2 planes and the magnetic field at ambient temperature. The cantilever was set inside a vacuum tight resin capsule filled at room temperature with ^{4}He gas to ensure thermalization of the sample. This capsule sits in the ^{3}He/^{4}He mixture of the dilution fridge. The temperature gradient between the sample located at the end of the cantilever and the thermometer located in the mixing chamber was estimated by measuring the critical field of a known compound under the same experimental conditions. The temperature gradient is about 0.2 ± 0.1 K at 0.4 K and negligible above 1 K. This uncertainty does not affect significantly the value of the physical parameters extracted from the data. The variation of the piezoresistance of the cantilever is measured with a Wheatstone bridge with an AC excitation at a frequency of 63 kHz.

For both electrical transport and torque measurements, we ensure that data collected during the rise and the fall of the field pulse are in perfect agreement, excluding any heating due to eddy currents.

3. Quantum oscillations in overdoped $Tl_2Ba_2CuO_{6+\delta}$

First experimental clues for the existence of a FS in overdoped $Tl_2Ba_2CuO_{6+\delta}$ came from AMRO [37] and ARPES [38] experiments. Both probes have suggested the existence of a FS in agreement with band structure calculations [39], e.g. a large quasi-two-dimensional (Q2D) warped cylinder which represents $\sim 65\%$ of the first Brillouin zone. Nevertheless AMRO is a semi-classical probe of the underlying FS which cannot directly conclude about the coherent nature of quasiparticles and the peak of quasiparticles measured by ARPES is too broad (100 meV) to be ascribed to coherent quasiparticles. Quantum oscillations are the most sensitive probe of the FS of a metal and demonstrate that well-defined quasiparticles are the low energy excitations of the system. They have long been searched for in overdoped cuprates, but have only been detected within the last two years.

[1] Note that m_s is renormalized by the spin-symmetric and the spin anti-symmetric (Stoner) parts of the electron–electron interactions but not by electron–phonon interactions. m^* is renormalized by the spin-symmetric part of the electron–electron interactions and also by electron–phonon interactions [34].

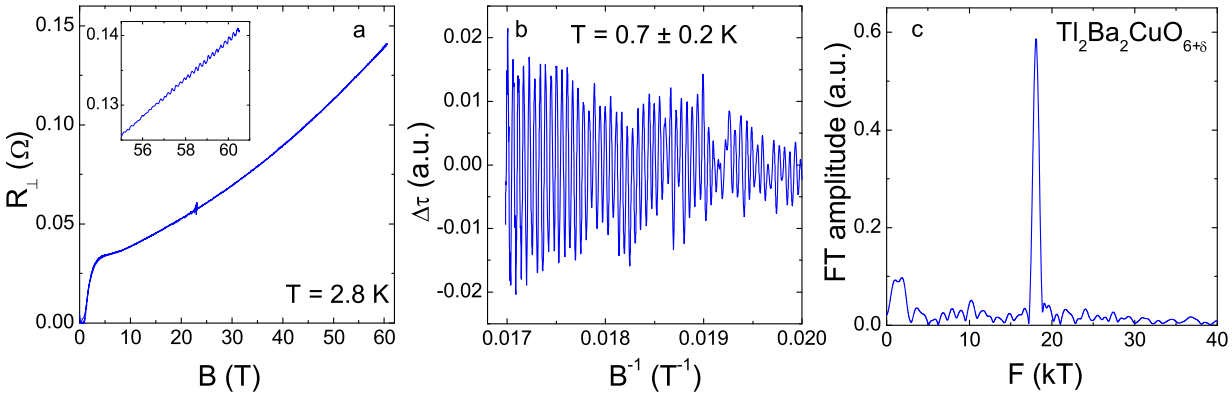

Fig. 2. (a) Magnetic field dependence of the interlayer resistance of overdoped $Tl_2Ba_2CuO_{6+\delta}$ ($T_c = 10$ K) at $T = 2.8$ K (raw data). The insert is a zoom on the high field part where quantum oscillations are seen for $B > 58$ T. (b) Oscillatory part of the torque data plotted as a function of $1/B$. (c) Fourier transform of the signal presented in (b), showing a single peak at $F = 18\,100$ T (from [40]).

Quantum oscillations measurements in overdoped $Tl_2Ba_2CuO_{6+\delta}$ were performed by means of longitudinal c-axis magnetoresistance as well as torque measurements [40]. Single crystals of $Tl_2Ba_2CuO_{6+\delta}$ with $T_c \approx 10$ K have been chosen for their high crystalline quality, with a mean free path estimated from zero field transport measurements to be of the order of 100 nm [5]. Fig. 2a shows the interlayer magnetoresistance up to 60 T. Above the superconducting transition, a strong magnetoresistance develops and quantum oscillations with small amplitude emerge above the noise level from 58 T in the magnetoresistance measurements (see insert of Fig. 2a). Fig. 2b displays the oscillatory part of the magnetization plotted versus $1/B$. The observation of oscillations, periodic in $1/B$, in both the magnetization and the resistivity, at fields well above the upper critical field, confirms these as quantum oscillations. The Fourier transform yields the power spectrum displayed in Fig. 2c which consists in a single sharp peak at a frequency of $18\,100 \pm 50$ T. The frequency of oscillation can be related to the extremal area of the FS perpendicular to the applied magnetic field via the Onsager relation, leading to a FS cross section $A_F = 172.8 \pm 0.5$ nm^{-2}. Assuming a cylindrical FS, the corresponding Fermi wavevector $k_F = 7.42 \pm 0.05$ nm^{-1} is in excellent agreement with the values deduced from AMRO ($k_F = 7.35 \pm 0.1$ nm^{-1}) [37] and ARPES (7.28 ± 0.2 nm^{-1}) [38] at similar doping level. The Luttinger sum rule states that at 2D the density of carriers $n = 2A_F/(2\pi)^2$, that is $n = F/\phi_0$ where $\phi_0 = h/2e$ is the flux quantum. The measured frequency corresponds to a carrier density $n = 1.3 = 1 + p$ with 1 hole corresponding to the half-filled band, and p hole added by hole doping. This agrees nicely with the Hall number $n_H = 1.3$ obtained at low temperature [5].

More recently, the angular dependence of quantum oscillations in two samples at different doping level ($T_c = 10$ K and 26 K) have been studied in static fields up to 45 T at the NHMFL [41]. The frequency reported for the $T_c = 10$ K sample is in excellent agreement with the one reported in pulsed field (18 100 T). The frequency of oscillations for the $T_c = 26$ K sample is 17 630 T, corresponding to a carrier density $n = 1.27 = 1 + p$.

The effective mass m^* of the quasiparticles can be deduced from the temperature dependence of the quantum oscillations amplitude. Within the experimental resolution, this evolution is found to follow the Lifshitz–Kosevich formalism. The deduced effective mass measured in pulsed field $m^* = (4.1 \pm 1)m_0$, where m_0 is the free electron mass, indicates that strong electronic correlations still persist at this doping level (DFT calculations predict that the bare band mass is 1.7 m_0 at this doping level) [42]. The lower temperature achieved in the static field study enables the effective mass deduced from the pulsed field experiment to be refined: $m^* = 4.9 - 5.8\ m_0$ for the $T_c = 10$ K samples and $m^* \approx 5\ m_0$ for the $T_c = 26$ K sample. Analysis of the field dependence of the quantum oscillations leads to an estimate of the Dingle temperature $T_D \approx 6$ K, corresponding to a mean free path $\ell \approx 320$ Å.

Given that for a two-dimensional FS, the electronic specific heat (Sommerfeld coefficient) is $\gamma_{el} = (\pi N_A k_B^2 a^2/3\hbar^2)m^*$ (where k_B is the Boltzmann constant, N_A is Avogadro number, and $a = 3.86$ Å is the in-plane lattice constant), m^* deduced from quantum oscillations converts to $\gamma_{el} = 7.6 \pm 0.6$ mJ mol^{-1} K^{-2} [42], in excellent agreement with that measured directly for overdoped polycrystalline $Tl_2Ba_2CuO_{6+\delta}$ (7.0 ± 2.0 mJ mol^{-1} K^{-2}) [43]. The mass enhancement appears to be rather doping independent in this doping range, as expected from the relatively doping independent Sommerfeld coefficient [43] extracted from heat capacity measurements.

We can thus make quantitative comparisons between quasiparticle properties derived from quantum oscillations at high fields and those measured directly by transport, ARPES and thermodynamics at zero field. This good overall consistency implies that the FS only consists of the single quasi-two-dimensional sheet measured with quantum oscillations.

The angular dependence of the amplitude of the oscillations is consistent with conventional Zeeman splitting, giving rise to spin zero at a polar angle $\theta = 27.5°$, yielding a spin mass of 4.9 m_0, close to the measured thermodynamic mass. This study also confirms that the crystals are highly homogeneous samples ($\delta p < 0.005$) and that quantum oscillations do not arise from a non-superconducting fraction of the sample, ruling out scenarios where the weakening of superconductivity with overdoping is due to inhomogeneity (i.e. phase segregation between hole-rich (non-SC) and hole-poor (SC)

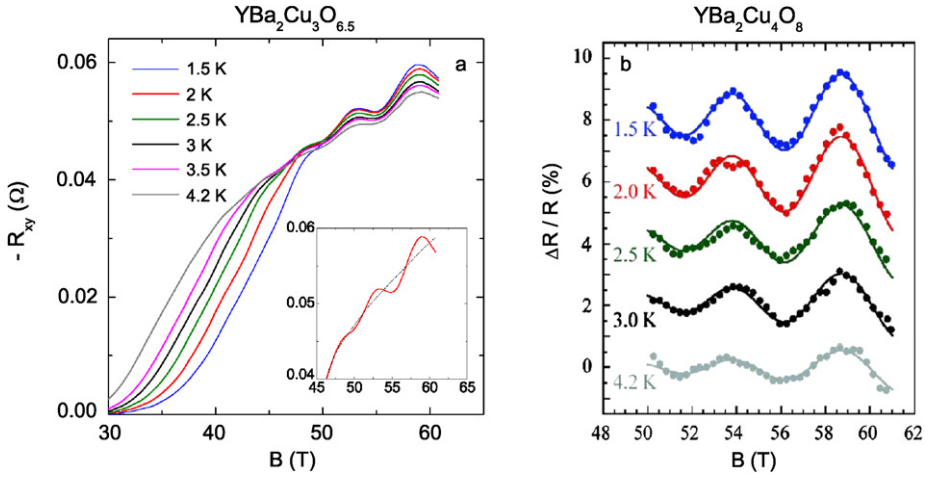

Fig. 3. (a) Hall resistance R_{xy} as a function of magnetic field B, for $YBa_2Cu_3O_{6.5}$, at different temperatures between 1.5 and 4.2 K (from [2]). The field is applied normal to the CuO_2 planes ($B \parallel c$) and the current is along the a-axis of the orthorhombic crystal structure ($J \parallel a$). Note that $R_{xy} < 0$, pointing to electron-like carriers. The insert shows a zoom on the data at $T = 2$ K, with a fitted monotonic background (dashed line). (b) The oscillatory component of the 4-points measurements of the magnetoresistance for $YBa_2Cu_4O_8$ at various temperatures. Solid lines are best fits to Eq. (1) giving $m^* = (2.7 \pm 0.3)m_0$ (from [44]).

regions). Superconductivity in $Tl_2Ba_2CuO_{6+\delta}$ is found disappear at $p(T_c = 0) = 0.31$, a significantly higher doping level than in $La_{2-x}Sr_xCuO_4$ where $p(T_c = 0) = 0.27$. Pair breaking effects due to impurity scattering can explain this trend as the amount of impurity and disorder is known to be greater in $La_{2-x}Sr_xCuO_4$.

In summary, the FS of overdoped $Tl_2Ba_2CuO_{6+\delta}$ is characterized by a large Q2D hole-like Fermi cylinder covering ∼65% of the first Brillouin zone. All the numbers deduced from these low temperature/high magnetic field studies are in excellent agreement with other experimental techniques (zero and low magnetic field) in the same material at similar doping levels. Despite strong electron–electron interactions, the observation of quantum oscillations implies that quasiparticles exist at all points of the FS of overdoped $Tl_2Ba_2CuO_{6+\delta}$. The observation of genuine quantum oscillations in $Tl_2Ba_2CuO_{6+\delta}$ supports the recognized idea that generalized Fermi-liquid theory can be applied on the overdoped side of the phase diagram, and that deviations from the Fermi–Dirac statistics are not relevant above 350 mK [42].

4. Quantum oscillations in underdoped $YBa_2Cu_3O_y$ and $YBa_2Cu_4O_8$

The open issue is now to understand how the large FS enclosing $1 + p$ holes for overdoped cuprates evolves as the system is driven closer to the Mott insulating phase. As shown by ARPES measurements for example, the underdoped regime is highly anomalous and the FS seems to consist of disconnected "Fermi arcs" [12]. The fundamental question that can be addressed with quantum oscillation measurements is whether underdoped copper oxides have a closed and coherent FS, and if so, whether it is different from that seen in the overdoped regime.

Fig. 3a shows the first convincing evidence of quantum oscillations in cuprates, detected in the Hall resistance of $YBa_2Cu_3O_{6.5}$ ($T_c = 57.5$ K, $p = 0.10$) where oscillations are clearly seen above the resistive superconducting transition [2]. The insert of Fig. 3a shows the 2 K isotherm and a smooth background curve (dashed line). A subtraction of this monotonic background allows to show that the oscillations are periodic in $1/B$, as expected for oscillations that arise from Landau quantization. The Fourier transform consists in a single peak at $F = (530 \pm 20)$ T. Oscillations of the same frequency are also observed in R_{xx}, albeit with a smaller amplitude [45]. The temperature dependence of the amplitude of the oscillations allows to deduce the effective mass $m^* = (1.9 \pm 0.1)m_0$. The observation of genuine quantum oscillations has been confirmed by measurements of the de Haas–van Alphen effect in $YBa_2Cu_3O_{6.5}$ [46] with the same frequency and effective mass. As a thermodynamic measurement, it firmly establishes the existence of well-defined quasiparticles at the FS with a substantial mean free path.

Fig. 3b shows the temperature dependence of the oscillatory component of the magnetoresistance for the related stoichiometric compound $YBa_2Cu_4O_8$ ($T_c = 82$ K, $p = 0.14$) between 50 and 61 T [44]. A fit of Eq. (1) to the data (shown in solid lines in Fig. 3b) gives a single frequency $F = (660 \pm 30)$ T, an effective mass $m^* = (2.7 \pm 0.3)m_0$ and an average SdH mean free path $\ell_{SdH} = (90 \pm 30)$ Å. Quantum oscillations in $YBa_2Cu_4O_8$ have also been observed using a tunnel-diode oscillator technique in pulsed magnetic fields up to 85 T in Los Alamos [47]. The oscillation frequency, $F = (660 \pm 15)$ T, and the effective mass, $m^* = (3.1 \pm 0.3)\ m_0$, are consistent with the measurements in Toulouse.

4.1. Evidence for multiple frequencies in $YBa_2Cu_3O_y$

The presence of the main frequency $F = 540$ T has been confirmed by de Haas–van Alphen measurements in $YBa_2Cu_3O_{6.5}$ (also grown at the University of British Columbia) by the Cambridge group in static magnetic fields up to 45 T in Tallahassee

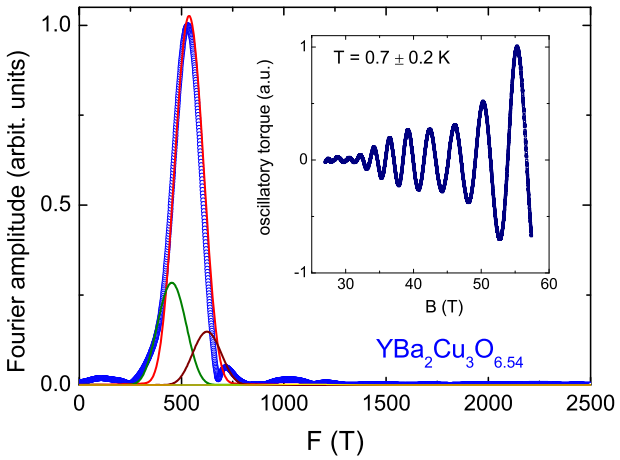

Fig. 4. Fourier analysis of the oscillatory torque (see insert) for $YBa_2Cu_3O_{6.54}$ showing that the main oscillation, at first believed to be single frequency, is composed of three closely spaced frequencies (from [49]).

[48]. In addition, a new oscillatory component of higher frequency called $F_\beta = (1650 \pm 40)$ T has been reported with an amplitude almost 30 times smaller than the dominant component. In order to confirm whether there are other closed sections of the FS, something of fundamental importance for clarifying the FS of HTSC in the pseudogap phase, we have performed high-precision measurements of the de Haas–van Alphen effect in underdoped $YBa_2Cu_3O_y$ ($y = 6.51$ and $y = 6.54$) by averaging several pulses (up to 10) for the same experimental conditions [49].

The insert of Fig. 4 shows the oscillatory component of the torque for $YBa_2Cu_3O_{6.54}$ at $T = (0.7 \pm 0.2)$ K. We found no evidence for an oscillatory component of the high frequency F_β as reported in Ref. [48]. However, the improved sensitivity of the measurements allows the discovery of some important details on the electronic structure of underdoped YBCO. While the amplitude of the oscillations should grow exponentially with magnetic field for a single frequency, a modulation of the amplitude of the oscillations (beating effect) can be noticed in the raw data, which is the signature of the presence of more than one frequency in the oscillatory spectrum. In order to resolve the multiple frequencies, we have performed fits of Eq. (1) to the data with four frequencies. Fig. 4 shows a Fourier transform of the data (the broad peak in blue circles with a maximum around 535 T) along with the relative amplitude of three frequencies used in the fit: a main frequency $F_1 = 540 \pm 15$ T (red line) and two satellites $F_2 = 450 \pm 15$ T (green line) and $F_3 = 630 \pm 40$ T (purple line). The fourth frequency $F_4 = 1130 \pm 20$ T corresponds probably to the second harmonic of F_1. The most natural explanation for the multiple frequencies is to invoke both a slight modulation of the FS sheet along the c-axis (warping) and a bilayer splitting effect, the latter being intrinsic to $YBa_2Cu_3O_y$ which contains two closely spaced CuO_2 planes.

In such a situation, angle dependent measurements are needed to clarify whether the multiple frequencies arise from a warped 3-dimensional surface or from separate Fermi sheets. Indeed, if the multiple frequencies arise from the neck and belly orbits, they should follow an angle dependence given by Eq. (2). c-axis longitudinal magnetoresistance measurements in $YBa_2Cu_3O_{6.5}$ have been performed at different angles between the CuO_2 plane and the magnetic field [33]. By measuring c-axis resistivity, this is the cyclotron motion of electrons in a plane perpendicular to the applied magnetic field which is being probed. The advantage of measuring c-axis resistivity is the large amplitude of the signal, which is at least two orders of magnitude larger than in-plane measurements due to the anisotropy of the electronic properties of $YBa_2Cu_3O_y$ and increases greatly the sensitivity of the measurements.

Assuming that the frequency splitting is due to warping of the FS, fits of Eq. (2) for a quasi-2D FS have been performed to the entire set of data. A method based on a genetic algorithm that explores a wide parameter space for the entire data set allows one to fit both the field and the angle dependence of the resistivity simultaneously and then iterating with fits to the field and temperature dependence [33]. The fitted model involves two surfaces ($F_{S1} = 526$ T and $F_{S2} = 478$ T) and their corresponding difference between the area of the neck and belly orbits ($\Delta F_{S1} = 3.5$ T and $\Delta F_{S2} = 37.7$ T). Note that the contributions from higher harmonics and a weak signal with a frequency near $F_3 = 630$ T have not been included in the model. The closeness in size of the cylinders, in the Dingle temperatures, and in the cyclotron masses suggest that the separate pieces of FS might be more closely related, as it is the case for example in a bilayer splitting scenario. In addition, these measurements uncover for the first time the effects of Zeeman splitting in the measurements [33], known as the spin-zero effect due to the interference of spin-up and spin-down contributions on each Fermi sheets. The spin-zero effect manifests itself as a vanishing of the amplitude of the oscillations for the entire field range at a specific angle. This indicates that the interaction of the magnetic field with the spins of the electrons is a simple symmetric Zeeman splitting, linear in magnetic field, a key sign that the quasiparticles in the cuprates behave as free spins. The presence of spin-zero is consistent with either non-magnetic scenarios [50] or longitudinal (or canted) spin density wave (SDW) (e.g. when the staggered moments have a substantial component along the field direction) [51].

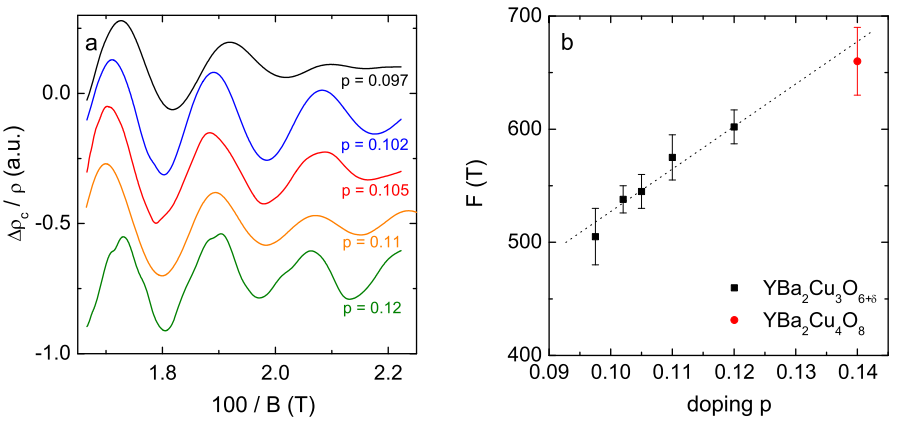

Fig. 5. (a) Oscillatory part of the c-axis magnetoresistance plotted as $1/B$ in $YBa_2Cu_3O_y$ at $T = 1.5$ K for different doping levels p. Note that the curves for $p = 0.102$ and $p = 0.105$ have been multiplied by a factor 10 and those for $p = 0.097$ and $p = 0.12$ by a factor 100. (b) Doping dependence of the frequency of quantum oscillations deduced from the raw data shown in (a). The red (round) point at $p = 0.14$ corresponds to in-plane resistivity measurements in $YBa_2Cu_4O_8$ from Ref. [44]. The dashed line is a guide to eyes.

4.2. Doping dependence of the frequency of quantum oscillations in $YBa_2Cu_3O_y$

A doping evolution of the frequency observed is of prime interest to settle the topology of the FS that will be discussed In Section 7. The oscillatory parts of the magnetoresistance of $YBa_2Cu_3O_y$ at five different doping levels between 45 T and 60 T is shown in Fig. 5. The signal becomes very small as the doping level departs from high quality oxygen ordered $YBa_2Cu_3O_{6.5}$ ($p = 0.11$).

While there is a subtle change in the frequency of oscillations, a careful analysis by indexing the maximum of the oscillations versus $1/B$ (Onsager relation [28]) yields the doping dependence of the frequency shown in Fig. 5b. There is a clear trend of increasing frequency as the doping increases, that is to say the size of the small Fermi pocket increases when the system is doped. This doping evolution is a key feature to discuss the topology of the FS in the underdoped regime and calls for a close theoretical investigation.

5. Comparison of quantum oscillations on both sides of the phase diagram

We now discuss the implications of quantum oscillations on both sides of the phase diagram of cuprates. In Fig. 6a, the oscillatory part of the magnetization for $YBa_2Cu_3O_{6.5}$ (red) and $Tl_2Ba_2CuO_{6+\delta}$ (magenta) are plotted together as $1/B$. There is a drastic difference in the frequency of the oscillations as shown by the corresponding Fourier transform in Fig. 6b. For overdoped $Tl_2Ba_2CuO_{6+\delta}$, a frequency $F = 18\,100$ T leads to a FS cross section area $A_F = 172.8$ nm^{-2}, which represents 65% of the first Brillouin zone. Surprisingly, the frequency $F = 540$ T found for underdoped $YBa_2Cu_3O_{6.5}$ corresponds to an extremal area $A_F = 5.1$ nm^{-2}, which represents only 1.9% of the first Brillouin zone. A sketch of the size of the pocket in the first Brillouin zone deduced from quantum oscillations is shown in the insert of Fig. 6b. For $Tl_2Ba_2CuO_{6+\delta}$, a frequency $F = 18\,100$ T converts to a carrier density $n = 1.3 = 1 + p$ carrier per Cu atom, while for $YBa_2Cu_3O_{6.5}$, the frequency $F = 540$ T corresponds to $n = 0.038$ carrier per planar Cu atom.

The dramatic difference between the small pocket revealed by the low frequency reported for $YBa_2Cu_3O_{6.5}$ and the large cylindrical surface observed in overdoped $Tl_2Ba_2CuO_{6+\delta}$ reflects thus the difference in the carrier density on both side of the phase diagram. The measurements offer strong support for the scenario that beyond a critical doping level p^* within the superconducting dome, cuprates undergo an FS reconstruction at a critical doping $0.14 < p^* < 0.27$, where the large hole-like FS reconstruct into small pockets. We will now show that the experimental findings in the underdoped regime are not compatible with band structure calculations and with doped Mott insulator scenarios.

5.1. Comparison with band structure calculations

Results obtained for overdoped $Tl_2Ba_2CuO_{6+\delta}$ are in excellent agreement with band structure calculations. For $YBa_2Cu_3O_{6.5}$, the FS deduced from band structure calculations consists of two large hole-like tubular CuO_2 sheets, plus three quasi-one-dimensional sheets. A subtle change in the Fermi energy can lead to the appearance of an additional small hole-like pocket [52], whose size may be comparable with the small pocket deduced from quantum oscillations. Few experimental observations rule out the FS derived from band structure calculations. The large tubular sheets have not been observed in any measurements. Moreover, if one assumes the small frequency corresponds to the small hole-like pocket at the Y point, it disagrees with the negative Hall effect (see Fig. 3a) which points to an electron pocket. Finally, band structure calculations in $YBa_2Cu_4O_8$ have shown that the CuO/BaO band which gives rise to the small hole-like pocket at the Y point in $YBa_2Cu_3O_{6.5}$, is 400 meV below the Fermi energy, excluding that this band could give rise to a small pocket

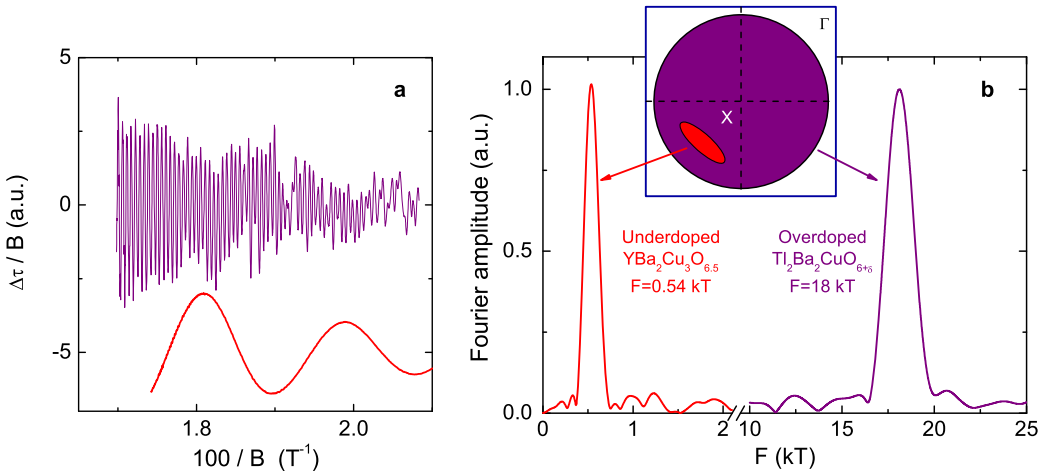

Fig. 6. (a) Oscillatory part of the magnetization (raw data) versus $1/B$ of $Tl_2Ba_2CuO_{6+\delta}$ (magenta) and $YBa_2Cu_3O_{6.5}$ (red). (b) Fourier analysis of the raw data shown in (a). The insert is a sketch of the size of the Fermi pocket in the first Brillouin zone deduced from the frequency of the quantum oscillations for $Tl_2Ba_2CuO_{6+\delta}$ (magenta) and $YBa_2Cu_3O_{6.5}$ (red). Note that the position in the Brillouin zone and the shape of the Fermi surfaces are arbitrary.

in $YBa_2Cu_4O_8$. We thus conclude that band structure calculations are incompatible with the measured quantum oscillations in both $YBa_2Cu_3O_{6.5}$ and $YBa_2Cu_4O_8$.

5.2. Four nodal hole pockets

A number of theories predict a FS made of four small hole-like pockets at nodal positions (carrier density equal to p) in the underdoped regime, going over to a large FS (carrier density equal to $1+p$) when p exceeds a critical value p^*. Some of these are analogous to the usual spin-density-wave scenario in the sense that they invoke the onset of an ordered phase with broken symmetry below p^* [20,21,24,53,54], while others do not require any broken symmetry [55–57]. The second class of scenarios predicts four-nodal hole pockets, whose area grows as the doping increases and merge into the large FS in the overdoped regime. Assuming that ARPES detects only one side of a hole pocket at $(\pi/2, \pi/2)$, e.g. that the quasiparticle residue for the part of the pocket facing (π, π) is rather small, these scenarios could reconcile the quantum oscillations with photoemission measurements [20,58,59]. Assuming that the pocket is a hole pocket (of arbitrary curvature) and there is nothing else in the FS, and assuming also that n must be equal to the density of doped holes ($n = p = 0.1$ for $YBa_2Cu_3O_{6.5}$), the Luttinger sum rule is clearly violated, whether the relevant Brillouin zone includes one or two of these pockets (whether $n = n_{SdH} = 0.038$ or $n = 2 \times n_{SdH} = 0.076$). In addition, the negative Hall coefficient R_H at low temperature (see Fig. 3a) implies that the Shubnikov–de Haas frequency must come from a high-mobility electron pocket, because the amplitude of Shubnikov–de Haas oscillations depends exponentially on mobility μ, as $\exp(-\pi/\mu B)$. Therefore, a scenario based on a doped Mott insulator which predicts a FS made of four nodal hole-like pockets, is not compatible with our experimental findings.

If the FS contains other sheets (not seen in the quantum oscillations measurements) besides the observed pockets, then the Luttinger sum rule can easily be satisfied. In particular, the negative Hall effect seen in Fig. 3a points to the presence of an electron pocket in the FS, arguing for a reconstruction of the local density approximation FS into small electron and hole sheets. Before discussing different theories based on the reconstruction of the FS, the next section will review evidence for the presence of an electron pocket in the FS of underdoped $YBa_2Cu_3O_y$.

6. The case for an electron pocket

6.1. Experimental evidences

The normal-state Hall coefficient $R_H = tR_{xy}/B$, where t is the sample thickness, measured at high field is displayed in Fig. 7a as a function of temperature for overdoped $Tl_2Ba_2CuO_{6+\delta}$ [5] ($p \approx 0.25$, green symbols), underdoped $YBa_2Cu_3O_{6.5}$ ($p = 0.097$, red symbols) and $YBa_2Cu_3O_{6.67}$ ($p = 0.12$, blue line) [60]. In overdoped $Tl_2Ba_2CuO_{6+\delta}$, the Hall coefficient is almost temperature independent and is positive (e.g. hole-like). It extrapolates to a small number corresponding to a large carrier density ($R_H = 1/ne$). However, for underdoped $YBa_2Cu_3O_y$, $R_H(T)$ goes from positive at high temperature to negative as $T \to 0$. As demonstrated in Refs. [60,62], the negative R_H is shown to be unambiguously a property of the normal state. The most natural explanation for the negative R_H is the presence of an electron pocket in the FS. In a scenario in which the FS contains both electron and hole sheets, the sign of R_H depends on the relative magnitude of the electron and hole densities n_e and n_h and mobilities μ_e and μ_h ($\mu = e\tau/m^*$). Given that these materials are hole-doped, we expect $n_h > n_e$. The fact that $R_H < 0$ at low temperature therefore implies that $\mu_e > \mu_h$ at low temperature. Given strong inelastic

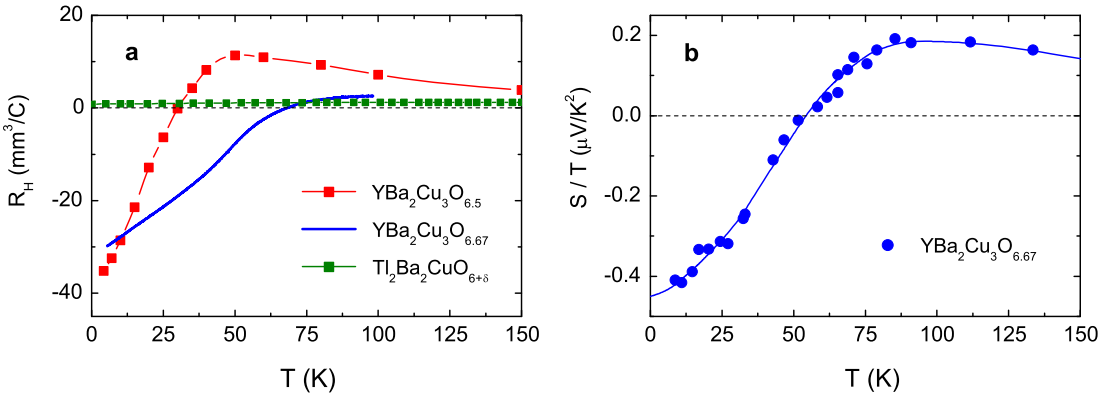

Fig. 7. (a) Hall coefficient R_H versus T for $YBa_2Cu_3O_{6.5}$ [60] (red symbols), $YBa_2Cu_3O_{6.67}$ [60] (blue line) and $Tl_2Ba_2CuO_{6+\delta}$ (green symbols) [5], at $B =$ 55, 45 and 16 T, respectively. (b) Thermopower of $YBa_2Cu_3O_{6.67}$ plotted as S/T versus T measured at $B = 28$ T [61].

scattering, this inequality can then easily be inverted at high temperature, offering a straightforward mechanism for the sign change in R_H.

The presence of an electron pocket in the FS of underdoped $YBa_2Cu_3O_y$ has been strengthened by Seebeck measurements in $YBa_2Cu_3O_{6.67}$ shown in Fig. 7b [61]. When a temperature difference ΔT is applied along the x-axis of a metallic sample, a longitudinal voltage V_x develops across the sample, and the Seebeck coefficient (or thermopower) is defined as $S = V_x/\Delta T$. In a Boltzmann picture for a single band metal, the magnitude of this coefficient is given by: $S/T = \pm\frac{\pi^2}{2}\frac{k_B}{e}\frac{1}{T_F}$ where $T_F = (\hbar^2/2k_B)(k_F^2/m^*)$ is the Fermi temperature. The sign of S is controlled by the carrier type: positive for holes, negative for electrons. We see that S/T undergoes a change of sign, from positive above $T = 50$ K to negative below, similar to the sign change of the Hall coefficient R_H. The fact that both S and R_H are negative in the normal state at $T \to 0$ is compelling evidence for an electron-like sheet in the FS. Moreover, the Fermi pocket measured by quantum oscillations has a sufficiently small Fermi energy to account for the large magnitude of the negative thermopower at $T \to 0$ [61].

Another evidence for the FS reconstruction into electron and hole sheets comes from the self-consistent analysis of the Hall resistivity and magnetoresistance of underdoped $YBa_2Cu_4O_8$ [63]. Field-independent fitting parameters ($n_{e,h}$ and $\mu_{e,h}$) are obtained at all temperatures between 1.5 and 100 K and for all fields above a cutoff field B_n that corresponds to the restoration of the resistive normal state. One important finding of this study is a dramatic fall in μ_h below 30 K which reveals a marked change in the mobility of the hole-like carriers, possibly due to their quasi-1D nature. It reflects the predominance of the electron pocket mobility at low temperature. Moreover, since the fitting parameters are field independent, this implies that if the FS reconstruction is field induced, it must take place at fields $B < B_n$.

In addition to the negative Hall and Seebeck coefficients at low temperature, another indication for the presence of an electron pocket in the FS of underdoped $YBa_2Cu_3O_y$ comes from the phase shift of about π between the quantum oscillations in the transverse magnetoresistance R_{xx} and in the Hall resistance R_{xy}, as noticed in Ref. [45]. Indeed, it has been shown that for a 2D electron gas, the diagonal and off-diagonal elements of the resistivity tensor oscillate in anti-phase as a function of the magnetic field [64].

6.2. Location of the electron pocket

As it will be discussed in Section 7, most scenarios based on FS reconstruction predict the emergence of an electron pocket at the anti-nodal directions of the Brillouin zone, i.e. at $(\pi, 0)$ and equivalents points. One way to probe the position of this pocket at $(\pi, 0)$ is to perform c-axis transport at low temperature. Indeed, in a simple tight binding model, the c-axis conductivity is proportional to $t_\perp$ and due to the particular structure of cuprates, the interlayer hopping integral $t_\perp$ depends strongly on the in-plane momentum $\mathbf{k}$ of carriers, namely for a tetragonal cuprate material [65]: $t_\perp(\mathbf{k}) = \frac{t_\perp}{4}[\cos(k_x a) - \cos(k_y a)]^2$. The c-axis hopping integral vanishes for momenta $\mathbf{k}$ along to the nodal directions ($k_x = k_y$) whereas it is maximal for momenta $\mathbf{k}$ along the anti-nodal directions ($k_x = 0$ or $k_y = 0$). The fact that strong quantum oscillations are observed in ρ_c [33] is a first indication that those states at $(\pi, 0)$ where $t_\perp$ is maximum, are in fact the small closed pocket responsible for the oscillations since the oscillatory part of the conductivity is proportional to $t_\perp$.

The presence of the electron pocket at $(\pi, 0)$ has also a pronounced impact on c-axis magnetotransport. Recent longitudinal c-axis resistivity ($I \parallel B \parallel c$) measurements in three underdoped samples of $YBa_2Cu_3O_y$ ($p = 0.097$, 0.109 and 0.120) up to 60 T and at low temperature have revealed that the c-axis resistivity is metallic-like at low temperature [66] in contrast to the insulating-like behaviour above T_c [67,68]. For all samples, the initial rise in the magnetoresistance-free ρ_c (extrapolated at $B = 0$ T) with decreasing temperature turns into a drop at low temperature, passing through a maximum between 20 and 40 K. This type of temperature dependence of the c-axis resistivity is the hallmark of a crossover between an incoherent regime at high temperature and a coherent regime at low temperature, as observed in numerous anisotropic quasi-two-dimensional systems such as Sr_2RuO_4 [69]. The metallic behavior of the c-axis resistivity at low temperature is

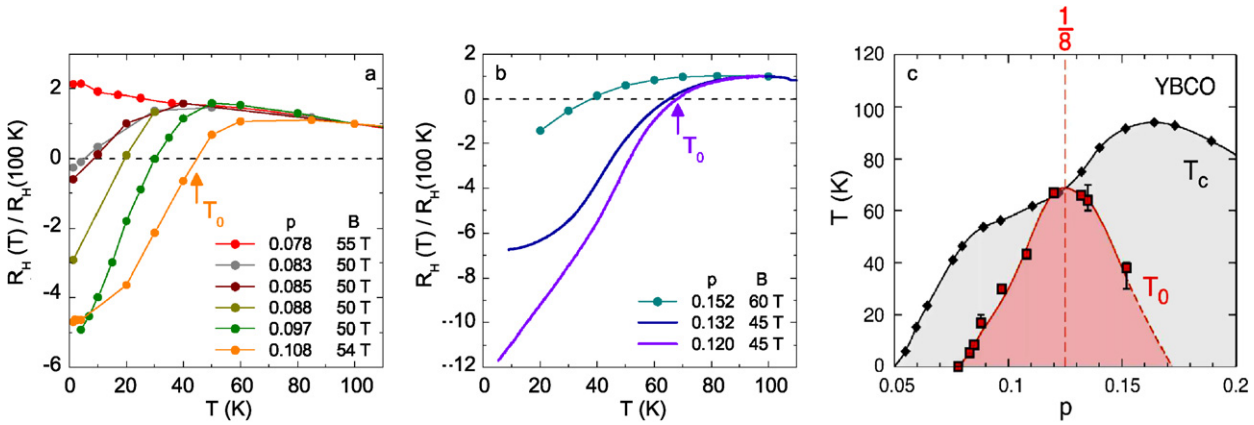

Fig. 8. Hall coefficient of $YBa_2Cu_3O_y$ at nine different dopings p as indicated, normalized to its value at $T = 100$ K. The data is taken at the highest magnetic field B reached, as indicated. (a) $p < 0.11$. (b) $p > 0.12$. T_0 marks the temperature at which $R_H(T)$ changes sign. (c) Phase diagram of YBCO, showing the zero-field superconducting transition temperature T_c (black diamonds) as a function of doping and the sign-change temperature T_0 of R_H, obtained once superconductivity is suppressed by a magnetic field, is shown in red squares (from [62]).

thus another strong indication of coherent states at $(\pi, 0)$ where most FS reconstruction scenarios predict the emergence of an electron pocket. The compensated electron and hole scenario [70] which ascribes the dominant frequency of the quantum oscillations to a *hole* pocket located at $(\pi/2, \pi/2)$ is not compatible with the present results which directly demonstrates that the dominant frequency arises from an electron pocket located at the anti-nodes. It is also difficult to reconcile such a scenario [70] with a large negative Hall coefficient [62].

6.3. Lifshitz transition

The doping dependence of the frequency linked to the electron pocket in Fig. 5 shows that the size of pocket decreases as the doping decreases. Unfortunately, probably due to sample quality, it has not been possible yet to observe quantum oscillations in $YBa_2Cu_3O_y$ below $p = 0.097$. In order to extract information on the electron pocket at lower doping, it is instructive to discuss the doping dependence of the Hall coefficient. Fig. 8(a) and (b) shows subsequent measurements of the normal-state Hall coefficient, measured at the highest field (between 45 and 60 T) as a function of temperature for several dopings from $p = 0.078$ to $p = 0.152$ [62]. These measurements confirm the trend of $R_H(T)$ going from positive at $T = 100$ K to negative as $T \to 0$ for all doping levels for $p > 0.08$. For $p = 0.078$, $R_H(T)$ never changes sign and simply increases monotonically with decreasing temperature. Fig. 8(c) shows the phase diagram for $YBa_2Cu_3O_y$ (T_c line in black symbols) where the characteristic temperature T_0, where the Hall effect changes sign, is plotted in red symbols [62]. We see that T_0 peaks at $p = 1/8$ and below this maximum, T_0 decreases monotonically (and linearly) to zero at $p = 0.08$. At this lowest doping, the vanishing of T_0 reflects the fact that R_H is seen positive at all temperatures (see data for the $p = 0.078$ sample in Fig. 8a). This drastic change of behavior in R_H points to a topological change in the FS of $YBa_2Cu_3O_y$ as the doping is decreased below a critical doping $p < p_L = 0.08$, a Lifshitz transition at which the closed electron pocket disappears.

Another impact of the disappearance the electron pocket can be inferred from the c-axis resistivity. Earlier measurements of c-axis transport on a $YBa_2Cu_3O_y$ sample with $T_c = 49$ K ($p \simeq 0.08$) [71] are consistent with such a transition: the magnetoresistance in $\rho_c(B)$ is entirely gone and $\rho_c(T)$ is incoherent, increasing down to the lowest temperatures. This close correlation between R_H and the magnetoresistance in ρ_c is further confirmation that the electron pocket in the FS of $YBa_2Cu_3O_y$ is located at $(\pi, 0)$ above a critical doping $p_L = 0.08$, where it controls how much of the orbital MR in the in-plane transport is reflected in the c-axis conduction.

7. Reconstruction of the FS of underdoped cuprates

As pointed out previously, the combination of a small FS volume from quantum oscillations and negative R_H and S pointing to electron pockets argues strongly for a reconstruction of the local density approximation FS, in both underdoped $YBa_2Cu_3O_y$ and $YBa_2Cu_4O_8$. The standard mechanism for such reconstruction is the onset of a density-wave instability [27]. In copper oxides, several mechanisms can be invoked for a reconstruction of the FS that would result in electron and hole surfaces.

7.1. Commensurate and incommensurate reconstruction

When an order induces a new periodicity in the system, the translational symmetry of the electronic states is broken. Any kind of order with a finite Q can produce a reconstruction of the FS. This order may in principle be a spin order (AF

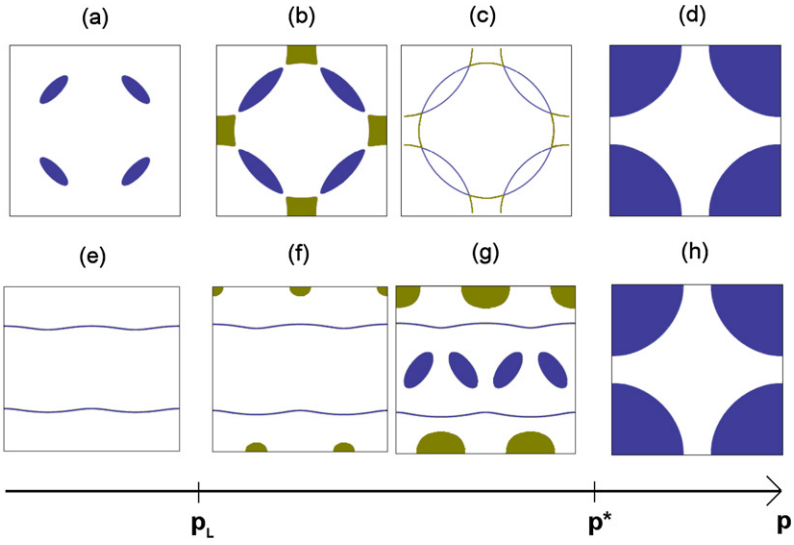

Fig. 9. (a) to (d) FS evolution appropriate for the hole-doped cuprates in a (π, π) ordering wavevector scenario (adapted from [21]). (e) to (h) FS evolution in the spin-stripe-ordered state (adapted from [72]). p^* marks a QCP where the FS starts to reconstruct. p_L marks the Lifshitz transition where the electron pocket disappears. Electron and hole sheets are depicted in dark yellow and blue, respectively.

or SDW), a charge order, a *d*-density wave order or a stripe order (a unidirectional and incommensurate modulation of spin and charge densities). Most theories focus on forms of order with a characteristic Q vector near (π, π). If $Q = (\pi, \pi)$, the reconstruction is said to be commensurate. If $Q = (\pi[1 \pm \delta], \pi)$, the reconstruction is incommensurate. This section will focus on commensurate and incommensurate AF, SDW and *d*-DW order, while the next section will be devoted to stripe order.

Several scenarios based on finite Q ordering wavevector lead to a reconstruction of the large hole-like FS into small hole pockets at $(\pi/2, \pi/2)$ and small electron pocket at $(\pi, 0)$ (see Fig. 9a–d for the commensurate case $\delta = 0$). A model based on an antiferromagnetic order has been proposed to explain the physical properties of electron-doped cuprates. ARPES measurements on $Nd_{2-x}Ce_xCuO_{4-\delta}$ [73] have seen the three Fermi-surface topologies sketched in Fig. 9 (but with a large electron pocket at $(\pi/2, \pi/2)$ and a small hole pocket at (π, π)). Such a model can also explain the sign change in the low-temperature Hall coefficient R_H measured in the electron-doped copper oxide $Pr_{2-x}Ce_xCuO_{4-\delta}$ (PCCO) [74], on crossing a critical concentration x_c close to where long-range antiferromagnetic order ends [53]. Quantum oscillations have been recently observed in the electron-doped $Nd_{2-x}Ce_xCuO_{4-\delta}$ [75] and reveal a sharp qualitative change in the FS topology at a critical doping level significantly exceeding the optimal doping.

Another approach is an antiferromagnetic SDW, a collective effect that emerges from the instability of the FS. SDW scenarios have been proposed soon after the discovery of HTSC (for a review, see Ref. [20]) and more recently, a theory taking into account the competition between superconductivity and SDW order has been developed [76,77]. While the normal state properties are controlled by a quantum critical point (QCP) at p_m linked to the onset of SDW order in a large FS metal, the competition between superconductivity and SDW order shifts the actual QCP to a lower doping $p_s < p_m$ in the underdoped regime, so that SDW order is only present for $p < p_s$ in the superconducting state. The normal state QCP at $p = p_m$ can be directly observed when the system remains metallic at $T = 0$ in the presence of a strong enough magnetic field. Note that a neutron scattering study of the static and dynamic spin correlations in the underdoped $YBa_2Cu_3O_{6.45}$ in magnetic fields up to 15 T have shown an enhancement of the static incommensurate magnetic order at low temperatures [78]. Whether SDW order would persist to higher doping in the presence of a large field that suppresses superconductivity, as it does in the case of LSCO [79], is not known yet for the case of $YBa_2Cu_3O_y$.

The neutron diffraction measurements in $YBa_2Cu_3O_{6.45}$ combined with the observation of the $F_\beta = 1650$ T frequency in Ref. [48] have led several authors to suggest a FS reconstruction with an incommensurate wavevector $Q = (\pi[1 \pm 2\delta], \pi)$, as it is the case for a collinear spin-density wave [80]. While this scenario makes a direct link between quantum oscillations measurements and incommensurate static order seen by neutron, the observation of the F_β frequency has not been confirmed as discussed above.

Another competing order scenario is based on an unusual broken symmetry *d*-density-wave order [24], which could also cause a (π, π) or incommensurate folding of the FS and could thus produce an electron pocket near $(\pi, 0)$ [81]. This state corresponds to circulating orbital currents arranged in a staggered pattern, leading to very small magnetic moments. No clear signature of *d*-DW order has been obtained using neutron diffraction.

The Lifshitz transition leading to the disappearance of the electron pocket is inherent to the commensurate (π, π) reconstruction scenario since the gap at the anti-nodal directions increases as the doping decreases. Such scenario can thus explain the Lifshitz transition at $p_L = 0.08$ but it remains to understand why the hole pocket is not seen in any

measurement. Moreover, the disappearance of the electron pocket below $p_L = 0.08$ is associated with a sudden jump in the magnitude of the in-plane resistivity (the so-called metal–insulator crossover) [62] and an increase in its in-plane anisotropy [82], which is not easy to reconcile with a (π, π) reconstruction scenario. We will see in the next section that the stripe order offers an alternative scenario able to explain both experimental observations.

7.2. Stripe order

In the low coupling limit [22,23,54], a stripe order consists of a combination of a charge density wave (potential V_c) and spin density wave (potential V_s), e.g. an oscillation of the charge density around its average value and a spin density modulation. The effect of stripe order is to reconstruct the large FS as shown for example in Fig. 9e–g for a doping $p = 1/8$, for different spin-stripe potential V_s and for the charge-stripe potential $V_c = 0$ [54,72]. The results are plotted not in the reduced Brillouin zone, but in a quadrant of the full square lattice zone. The generic FS is complicated since it consists of open orbits and depending on the value of the charge and spin scattering potentials, of hole pockets (nodal directions), and electron pockets (anti-nodal directions). It is noteworthy that in the model of Ref. [54] a condition for the appearance of an electron pocket in the reconstructed FS is to have a spin potential V_s non-zero. This scenario could in principle explain the presence of only one frequency (and the related ones due to bilayer splitting and warping of the FS) if the FS contains only the electron pocket and the 1D chains, as the one shown in Fig. 9f. Due to the presence of the 1D chains, the Luttinger sum rule can easily be satisfied since quantum oscillations detect only the closed orbit. A strong indication for a stripe scenario comes from the in-plane resistivity of $YBa_2Cu_3O_y$ at $p < 0.08$ whose anisotropy increases at low temperature, reaching an anisotropy ratio $\rho_a/\rho_b = 2$ [82]. This means that in the metallic state below the critical doping $p_L = 0.08$, the FS that remains after the electron pocket has disappeared must have anisotropy in the plane, as one expect if the FS consists of only 1D chains. Norman et al. have shown that a Lifshitz transition, where the pockets touch and so connect to form an open (quasi-1D) FS (see Fig. 9e–f), occurs at a doping level p_L comparable to that observed in experiment. Note that in this model, the authors have assumed that the incommensurability of the stripe wavevector depends on the doping level and that the size of the electron pocket is independent of doping, whereas our study suggests that the size of the FS slightly increases as the doping increases from $p = 0.097$ to 0.14. A consequence of the Lifshitz transition is the manifestation of the so-called metal–insulator crossover. There is a sudden change in behavior occurring between $p = 0.08$ and $p = 0.09$, where ρ_a (100 K) jumps from a low, p-independent value above $p = 0.09$ to a high, strongly p-dependent value below $p = 0.08$ [62]. This metal–insulator crossover can be explained by the disappearance of the electron pocket, leaving only the quasi-1D sheets of the FS which have a much lower conductivity at low temperature.

In another stripe model, which assumes a substantial C_4 symmetry breaking, a charge density wave order can produce an electron pocket close to the anti-node [83]. This model has been developed in order to reconcile the charge density modulation observed at low temperature by recent NMR measurements, without any form of SDW order [84].

A stripe scenario appears thus quite reasonable for $YBa_2Cu_3O_y$: it can account for the appearance of an electron pocket in the FS below p^*, a result of broken translational symmetry, and for its disappearance at p_L, due to a Lifshitz transition. It is also consistent with the evidence of broken rotational symmetry from resistivity [82] and recent Nernst measurements [16].

A recent comparison of Seebeck data in $YBa_2Cu_3O_y$ and in $La_{1.8-x}Eu_{0.2}Sr_xCuO_4$, a material where stripe order at low temperature is well established, reveals a detailed similarity as a function of both doping and temperature, which shows that: 1) the two very different cuprate materials undergo the same Fermi-surface reconstruction; 2) this reconstruction is caused by stripe order [85].

8. Conclusion

After two decades of intense theoretical as well as experimental efforts to understand how high temperature superconductivity sets in and how to describe the normal state properties, the observation of quantum oscillation has deeply changed the landscape to describe these fascinating materials. It allows to discuss a fundamental concept in metals, the FS, and therefore about the normal state with new theoretical background. The measurements of quantum oscillations at low temperature on both sides of the phase diagram of cuprates confirm the existence of a FS with sharply defined excitations on the overdoped side but also show that the FS has suffered a drastic modification on the underdoped side. The small Fermi pocket inferred from quantum oscillations in the underdoped regime, combined with the negative Hall and Seebeck coefficients pointing to an electron pocket greatly strengthens the case that the FS of $YBa_2Cu_3O_y$ undergoes a reconstruction because the translational symmetry of its lattice is broken at low temperature. The fact that strong quantum oscillations are observed in ρ_c and the observation of a crossover towards a coherent regime in the c-axis resistivity at low temperature implies that this electron pocket is located at the anti-nodal directions in the first Brillouin zone, as predicted by most density-wave scenarios. Among all these scenarios (antiferromagnetic, spin density wave, d-DW and stripes), the stripe scenario seems to be the most adequate to describe most of the experimental findings obtained from various transport probes including the rotational symmetry breaking at T^*. Of course, this order parameter which breaks the translational symmetry of the lattice is not yet settled in $YBa_2Cu_3O_y$ and several measurements can help resolving this issue such as a full doping dependence of quantum oscillations, neutron, NMR and X-ray measurements in high fields.

Acknowledgements

The authors would like to thank many colleagues for fruitful discussions. We also acknowledge the technical support from the staff of the LNCMI-Toulouse. Part of this work was supported by the French ANR DELICE and FP7 I3 EuroMagNET II. L.T. and N.D.L. acknowledge support from CIFAR, NSERC, CFI, and FQRNT; R.L., D.A.B. and W.N.H. acknowledge support from CIFAR and NSERC; N.E.H. and A.C. acknowledge support from the EPSRC (UK) and the Royal Society.

References

[1] J.G. Bednorz, K.A. Müller, Z. Phys. B Condens. Matter 64 (1986) 189–193.
[2] N. Doiron-Leyraud, C. Proust, D. LeBoeuf, J. Levallois, J.-B. Bonnemaison, R. Liang, D.A. Bonn, W.N. Hardy, L. Taillefer, Nature 447 (2007) 565–568.
[3] C. Proust, E. Boaknin, R.W. Hill, L. Taillefer, A.P. Mackenzie, Phys. Rev. Lett. 89 (2002) 147003.
[4] S. Nakamae, K. Behnia, N. Mangkorntong, M. Nohara, H. Takagi, S.J.C. Yates, N.E. Hussey, Phys. Rev. B 68 (2003) 100502(R).
[5] A.P. Mackenzie, S.R. Julian, D.C. Sinclair, C.T. Lin, Phys. Rev. B 53 (1996) 5848.
[6] T. Manako, Y. Kubo, Y. Shimakawa, Phys. Rev. B 46 (1992) 11019.
[7] M. Abdel-Jawad, J.G. Analytis, L. Balicas, A. Carrington, J.P.H. Charmant, M.M.J. French, N.E. Hussey, Phys. Rev. Lett. 99 (10) (2007) 107002.
[8] R. Daou, N. Doiron-Leyraud, D. LeBoeuf, S.Y. Li, F. Laliberté, O. Cyr-Choinière, Y.J. Jo, L. Balicas, J.-Q. Yan, J.-S. Zhou, J.B. Goodenough, L. Taillefer, Nature Phys. 5 (2009) 31.
[9] R.A. Cooper, Y. Wang, B. Vignolle, O.J. Lipscombe, S.M. Hayden, Y. Tanabe, T. Adachi, Y. Koike, M. Nohara, H. Takagi, C. Proust, N.E. Hussey, Science 323 (2009) 603.
[10] W.W. Warren, R.E. Walstedt, G.F. Brennert, R.J. Cava, R. Tycko, R.F. Bell, G. Dabbagh, Phys. Rev. Lett. 62 (1989) 1193.
[11] H. Alloul, T. Ohno, P. Mendels, Phys. Rev. Lett. 63 (1989) 1700.
[12] M.R. Norman, H. Ding, M. Randeria, J.C. Campuzano, T. Yokoya, T. Takeuchi, T. Takahashi, T. Mochiku, K. Kadowaki, P. Guptasarma, D.G. Hinks, Nature 392 (1998) 157.
[13] B. Fauqué, Y. Sidis, V. Hinkov, S. Pailhès, C.T. Lin, X. Chaud, P. Bourges, Phys. Rev. Lett. 96 (2006) 197001.
[14] Y. Li, V. Balédent, N. Barisic, Y. Cho, B. Fauqué, Y. Sidis, G. Yu, X. Zhao, P. Bourges, M. Greven, Nature 455 (2008) 372.
[15] J. Xia, E. Schemm, G. Deutscher, S.A. Kivelson, D.A. Bonn, W.N. Hardy, R. Liang, W. Siemons, G. Koster, M.M. Fejer, A. Kapitulnik, Phys. Rev. Lett. 100 (2008) 127002.
[16] R. Daou, J. Chang, D. LeBoeuf, O. Cyr-Choinière, F. Laliberté, N. Doiron-Leyraud, B.J. Ramshaw, R. Liang, D.A. Bonn, W.N. Hardy, L. Taillefer, Nature 463 (2010) 519.
[17] M.R. Norman, D. Pines, C. Kallin, Adv. Phys. 54 (2005) 715.
[18] P.W. Anderson, Science 235 (1987) 1196.
[19] V.J. Emery, S.A. Kivelson, Nature 374 (1995) 434.
[20] A.V. Chubukov, D.K. Morr, Phys. Rep. 288 (1997) 355.
[21] E.G. Moon, S. Sachdev, Phys. Rev. B 80 (2009) 035117.
[22] S.A. Kivelson, I.P. Bindloss, E. Fradkin, V. Oganesyan, J.M. Tranquada, A. Kapitulnik, C. Howald, Rev. Mod. Phys. 75 (2003) 1201.
[23] M. Vojta, Adv. Phys. 58 (2009) 699.
[24] S. Chakravarty, R.B. Laughlin, D.K. Morr, C. Nayak, Phys. Rev. B 63 (2001) 094503.
[25] C.M. Varma, Phys. Rev. B 55 (1997) 14554.
[26] J.L. Tallon, J.W. Loram, Physica C 349 (2001) 53.
[27] L. Taillefer, J. Phys.: Condens. Matt. 21 (2009) 164212.
[28] D. Shoenberg, Magnetic Oscillations in Metals, Cambridge Univ. Press, Cambridge, 1984.
[29] W.J. de Haas, P.M. van Alphen, Proc. Sect. Sci. K. Ned. Akad. Wet. 33 (1930) 1106.
[30] L. Shubnikov, W.Y. de Haas, Comm. Phys. Lab. Univ. Leiden 207a, 207c, 207d, 210a.
[31] I.M. Lifshitz, A.M. Kosevich, Zh. Eksp. Teor. Fiz. 29 (1955) 730.
[32] F.E. Richards, Phys. Rev. B 8 (1973) 2552.
[33] B.J. Ramshaw, B. Vignolle, J. Day, R. Liang, W. Hardy, C. Proust, D.A. Bonn, Nature Phys. 7 (2011) 234.
[34] C. Bergemann, A.P. Mackenzie, S.R. Julian, D. Forsythe, E. Ohmichi, Adv. Phys. 52 (2003) 639.
[35] P. Frings, J. Billette, J. Béard, O. Portugall, F. Lecouturier, G.L.J.A. Rikken, IEEE Trans. Appl. Supercond. 18 (2008) 592.
[36] E. Ohmichi, T. Osada, Rev. Sci. Instrum. 73 (2002) 3022.
[37] N.E. Hussey, M. Abdel-Jawad, A. Carrington, A.P. Mackenzie, L. Balicas, Nature 425 (2003) 814.
[38] M. Platé, J.D.F. Mottershead, I.S. Elfimov, D.C. Peets, R. Liang, D.A. Bonn, W.N. Hardy, S. Chiuzbaian, M. Falub, M. Shi, L. Patthey, A. Damascelli, Phys. Rev. Lett. 95 (2005) 077001.
[39] D.J. Singh, W.E. Pickett, Physica C 203 (1992) 193.
[40] B. Vignolle, A. Carrington, R.A. Cooper, M.M.J. French, A.P. Mackenzie, C. Jaudet, D. Vignolles, C. Proust, N.E. Hussey, Nature 455 (2008) 952.
[41] A.F. Bangura, P. Rourke, T. Benseman, M. Matusiak, J. Cooper, N. Hussey, A. Carrington, Phys. Rev. B 82 (2010) 140501(R).
[42] P.M.C. Rourke, A.F. Bangura, T.M. Benseman, M. Matusiak, J.R. Cooper, A. Carrington, N.E. Hussey, New J. Phys. 12 (2010) 105009.
[43] J.W. Loram, K.A. Mirza, J.M. Wade, J.R. Cooper, W.Y. Liang, Physica C 235–240 (1994) 134.
[44] A.F. Bangura, J.D. Fletcher, A. Carrington, J. Levallois, M. Nardone, B. Vignolle, P.J. Heard, N. Doiron-Leyraud, D. LeBoeuf, L. Taillefer, S. Adachi, C. Proust, N.E. Hussey, Phys. Rev. Lett. 100 (2008) 047004.
[45] C. Jaudet, J. Levallois, A. Audouard, D. Vignolles, B. Vignolle, R. Liang, D. Bonn, W. Hardy, N. Hussey, L. Taillefer, C. Proust, Physica B 404 (2009) 354.
[46] C. Jaudet, D. Vignolles, A. Audouard, J. Levallois, D. LeBoeuf, N. Doiron-Leyraud, B. Vignolle, M. Nardone, A. Zitouni, R. Liang, D.A. Bonn, W.N. Hardy, L. Taillefer, C. Proust, Phys. Rev. Lett. 100 (2008) 187005.
[47] E.A. Yelland, J. Singleton, C.H. Mielke, N. Harrison, F.F. Balakirev, B. Dabrowski, J.R. Cooper, Phys. Rev. Lett. 100 (2008) 047003.
[48] S.E. Sebastian, N. Harrison, E. Palm, T.P. Murphy, C.H. Mielke, R. Liang, D.A. Bonn, W.N. Hardy, G.G. Lonzarich, Nature 454 (2008) 200.
[49] A. Audouard, C. Jaudet, D. Vignolles, R. Liang, D.A. Bonn, W.N. Hardy, L. Taillefer, C. Proust, Phys. Rev. Lett. 103 (2009) 157003.
[50] S. Chakravarty, D. Garcia-Aldea, Phys. Rev. B 82 (2010) 184526.
[51] M.R. Norman, J. Lin, Phys. Rev. B 82 (2010) 060509(R).
[52] A. Carrington, E.A. Yelland, Phys. Rev. B 76 (2007) 140508.
[53] J. Lin, A.J. Millis, Phys. Rev. B 72 (2005) 214506.
[54] A. Millis, M.R. Norman, Phys. Rev. B 76 (2007) 220503.
[55] K.-Y. Yang, T.M. Rice, F.-C. Zhang, Phys. Rev. B 73 (2006) 174501.
[56] P.A. Lee, Rep. Progr. Phys. 71 (2008) 012501.

[57] T.D. Stanescu, G. Kotliar, Phys. Rev. B 74 (2006) 125110.
[58] N. Harrison, R.D. McDonald, J. Singleton, Phys. Rev. Lett. 99 (2007) 206406.
[59] S. Chakravarty, C. Nayak, S. Tewari, Phys. Rev. B 68 (2003) 100504.
[60] D. LeBoeuf, N. Doiron-Leyraud, J. Levallois, R. Daou, J.-B. Bonnemaison, N.E. Hussey, L. Balicas, B.J. Ramshaw, R. Liang, D.A. Bonn, W.N. Hardy, S. Adachi, C. Proust, L. Taillefer, Nature 450 (2007) 533.
[61] J. Chang, R. Daou, C. Proust, D. LeBoeuf, N. Doiron-Leyraud, F. Laliberté, B. Pingault, B.J. Ramshaw, R. Liang, D.A. Bonn, W.N. Hardy, H. Takagi, A.B. Antunes, I. Sheikin, K. Behnia, L. Taillefer, Phys. Rev. Lett. 104 (2010) 057005.
[62] D. LeBoeuf, N. Doiron-Leyraud, B. Vignolle, M. Sutherland, B.J. Ramshaw, J. Levallois, R. Daou, F. Laliberté, O. Cyr-Choinière, J. Chang, Y.J. Jo, L. Balicas, R. Liang, D.A. Bonn, W.N. Hardy, C. Proust, L. Taillefer, Phys. Rev. B 83 (2011) 054506.
[63] P.M.C. Rourke, A.F. Bangura, C. Proust, J. Levallois, N. Doiron-Leyraud, D. LeBoeuf, L. Taillefer, S. Adachi, M.L. Sutherland, N.E. Hussey, Phys. Rev. B 82 (2010) 020514(R).
[64] T. Ando, J. Phys. Soc. Jpn. 37 (1974) 1233.
[65] S. Chakravarty, A. Sudbo, P.W. Anderson, S. Strong, Science 261 (1993) 337.
[66] B. Vignolle, B.J. Ramshaw, J. Day, D. LeBoeuf, W. Hardy, R. Liang, D. Bonn, L. Taillefer, C. Proust, unpublished.
[67] S.L. Cooper, K.E. Gray, in: D.M. Ginsberg (Ed.), Physical Properties of High Temperature Superconductors IV, World Scientific, Singapore, 1994, pp. 61–188.
[68] D.G. Clarke, S.P. Strong, Adv. Phys. 46 (1997) 545.
[69] N.E. Hussey, A.P. Mackenzie, J.R. Cooper, Y. Maeno, S. Nishizaki, T. Fujita, Phys. Rev. B 57 (1998) 5505.
[70] S.E. Sebastian, N. Harrison, P.A. Goddard, M.M. Altarawneh, C.H. Mielke, R. Liang, D.A. Bonn, W.N. Hardy, O. Andersen, G.G. Lonzarich, Phys. Rev. B 81 (2010) 214524.
[71] F. Balakirev, Y. Ando, A. Passner, J. Betts, L. Schneemeyer, K. Segawa, G. Boebinger, Physica C 341–348 (2000) 1877.
[72] J. Lin, A.J. Millis, Phys. Rev. B 78 (2008) 115108.
[73] N.P. Armitage, F. Ronning, D.H. Lu, C. Kim, A. Damascelli, K.M. Shen, D.L. Feng, H. Eisaki, Z.-X. Shen, P.K. Mang, N. Kaneko, M. Greven, Y. Onose, Y. Taguchi, Y. Tokura, Phys. Rev. Lett. 88 (2002) 257001.
[74] Y. Dagan, M.M. Qazilbash, C.P. Hill, V.N. Kulkarni, R.L. Greene, Phys. Rev. Lett. 92 (2004) 167001.
[75] T. Helm, M.V. Kartsovnik, M. Bartkowiak, N. Bittner, M. Lambacher, A. Erb, J. Wosnitza, R. Gross, Phys. Rev. Lett. 103 (2009) 157002.
[76] E. Demler, S. Sachdev, Y. Zhang, Phys. Rev. Lett. 87 (2001) 067202.
[77] S. Sachdev, Phys. Stat. Sol. B 247 (2010) 537.
[78] D. Haug, V. Hinkov, A. Suchaneck, D.S. Inosov, N.B. Christensen, C. Niedermayer, P. Bourges, Y. Sidis, J.T. Park, A. Ivanov, C.T. Lin, J. Mesot, B. Keimer, Phys. Rev. Lett. 103 (2009) 017001.
[79] B. Lake, H.M. Rønnow, N.B. Christensen, G. Aeppli, K. Lefmann, D.F. McMorrow, P. Vorderwisch, P. Smeibidl, N. Mangkorntong, T. Sasagawa, M. Nohara, H. Takagi, T.E. Mason, Nature 415 (2002) 299.
[80] N. Harrison, Phys. Rev. Lett. 102 (2009) 206405.
[81] S. Chakravarty, H.-Y. Kee, Proc. Natl. Acad. Sci. 105 (2008) 8835.
[82] Y. Ando, K. Segawa, S. Komiya, A.N. Lavrov, Phys. Rev. Lett. 88 (2002) 137005.
[83] H. Yao, D. Lee, S. Kivelson, arXiv:1103.2115.
[84] T. Wu, H. Mayaffre, S. Kramer, M. Horvatic, C. Berthier, W.N. Hardy, R. Liang, D.A. Bonn, M.-H. Julien, unpublished.
[85] F. Laliberté, J. Chang, N. Doiron-Leyraud, E. Hassinger, R. Daou, M. Rondeau, B.J. Ramshaw, R. Liang, D.A. Bonn, W.N. Hardy, S. Pyon, T. Takayama, H. Takagi, I. Sheikin, L. Malone, C. Proust, K. Behnia, L. Taillefer, arXiv:1102.0984.